Anchorage effect of bolt on en-echelon fractures: a comparison between energy-absorbing bolt and conventional rigid bolt

Yuanchao Zhang[a], Yujing Jiang[a*], Zhi Wang[a], Qian Yin[b], Miao Chen[c]

a. Graduate School of Engineering, Nagasaki University, Nagasaki 852-8521, Japan

b. State Key Laboratory for Geomechanics and Deep Underground Engineering, China University of Mining and Technology, Xuzhou 221116, China

c. College of Energy and Mining Engineering, Shandong University of Science and Technology, Qingdao 266590, China

Abstract Widespread en-echelon fractures may induce some disasters such as landslides of rock slopes and destabilization of underground excavations. Bolt support has been widely used in various rock engineerings for many years, but the bolting behavior of en-echelon fractures has rarely been studied. In this study, the anchorage effect of conventional rigid bolt and energy-absorbing bolt was investigated by direct shear tests under constant normal stiffness conditions. The bolting performance of the two bolts was quantitatively evaluated based on shear strength and dilation indices. The test results show that the anchorage effect of bolt is closely related to the bolt material and fracture angle. This is essentially determined by the deformation mechanism of bolt in different shear failure structures. A bolt deformation factor was proposed to predict the breakage displacement of bolt at different fracture angles and a bolt contribution index was defined to comprehensively evaluate the bolting performance.

Keywords Anchorage effect En-echelon fractures Shear failure structure Energy-absorbing bolt

***Corresponding author:**
Professor **Yujing Jiang**
E-mail address: jiang@nagasaki-u.ac.jp
School of Engineering, Nagasaki University, 1-14 Bunkyo-machi, Nagasaki 8528521, Japan

1 Introduction

Natural rock masses usually exhibit obvious discontinuities due to the presence of weak structures with different scales such as joints, fissures, bedding planes and faults, which are formed during a long geological history. The geometric and mechanical properties of these discontinuities greatly affect the strength and deformation of rock masses and are therefore critical to engineering design. En-echelon fractures as a typical discontinuous geological structure, appearing as parallel or subparallel, overlapping or step-like, can be frequently observed in various rock engineerings such as mines, tunnels, slopes, etc. [1-6]. The formation of en-echelon fractures is essentially due to the localised extension that occurs inside the shear zone and reflects the progressive damage process of the rock mass [7]. Depending on the relationship between the main fault and the shear motion, en-echelon fractures typically exhibit different geometrical structure (dip, spacing and distribution) in different tip damage zones [8-10]. Influenced by tectonic history, excavation disturbance or seismic activity, the en-echelon fractures gradually cracks and eventually forms a through-going slip zone by destroying the rock bridges. For example, a hourglass structure formed by en-echelon fractures was observed in the yield pillars in underground mines [1]. Landslides caused by the step-path failure of en-echelon fractures were reported in Aishihik River [3] and Xiaowan hydroelectric station in China [4], see Fig. 1(a). The pull-aparts zones between the interacting tips of en-echelon fractures can be clearly observed at the outcrops in Marsalforn, Gozo Island [9,10].

In order to avoid rock mass instability caused by the activation of pre-existing fractures, many reinforcement methods are used to strengthen the rock mass, of which bolt support is the most commonly used in rock slopes and underground engineerings [11-13], as shown in Fig. 1(b). In the past decades, the anchorage effect of bolts has been extensively studied based on laboratory tests. For example, Jing et al. [14] performed uniaxial compression tests on a large-scale jointed rock mass with different joint angles. Their results show that the anchorage strength of jointed rock masses is higher than that without bolts and the reinforcement effect depends highly on the joint angle and the number of bolts. Li et al. [15] further concluded from biaxial compression tests that the anchoring effect of bolts decreases with increasing lateral pressure. Meng et al. [16] investigated the shear behavior of bolted rock mass using an oblique shear apparatus and concluded that the full-length grouted bolts significantly reduce post-peak brittle failure and increase the residual strength of the rock mass. Jalalifar and Aziz [17] performed double-shear tests on bolted concrete specimens and concluded that the pretension loads of the bolt has an important effect on the shear resistance, shear displacement, and failure mechanism of the bolted specimens. Wang et al. [18] further confirmed by field tests that the increased pre-tightening force can improve the control effect on the surrounding rock mass. Yang et al. [19] explored in detail the fracturing and anchoring mechanism of jointed rock mass on a microscopic scale using digital speckle correlation method, acoustic emission technique and X-ray CT observations. Wang et al. [20] investigated the shear behavior of bolted jointed rock-like specimens with different roughness and bolt elongation. They concluded that the shear strength of jointed rock mass increased with the roughness of the joint surface, while decreasing with the increase of the bolt elongation. Wu et al. [21,22] performed cycle shear tests on the bolted rock joint and found that the cyclic shear loading especially with a large cyclic displacement plays an important role on the shear performance of the rock bolt. And, the energy-absorbing rock bolt behaves better than the fully encapsulated rock bolt under cyclic shear conditions. Skrzypkowski et al. found that for a rock mass, which is prone to emit seismic energy in the form of tremors and which is characterized by high stratification, a yielding bolt support is selected equipped with either disc springs [23] or with special dome bearing plates [24]. In addition, many other factors have also been studied regarding the shear behavior of bolted joints, such as bolt material [25], bolt type [26,27], bolt surface profile and rock strength [28], bolt diameter and normal pressure [29].

In recent years, with the development of rock engineerings to the deep earth, the complex deep environment characterized by high ground stress, high seepage pressure and high ground temperature has posed new challenges to the conventional bolt support [30,31]. In order to adapt to the large deformation characteristics of deep rock mass, energy-absorbing bolts have been developed rapidly. Energy-absorbing bolt can provide constant resistance during the deformation of the surrounding rock mass and shows a large elongation, making it better adapted to engineering rock masses subjected to impact loads, such as rock bursts and excavation blasting [32-34]. The high elongation of energy-absorbing rock bolt is generally achieved by adding special slip components (structural components sliding type) or changing the material properties of the bolt rod (steel deformation type). For example, the famous He bolt [30, 31], as a typical energy-absorbing bolt, achieves an extraordinarily large elongation and high constant resistance through a designed compound structure consisting of a cone-like piston sliding inside an elastically-deformable sleeve pipe. Several other types of energy-absorbing bolts have also been developed and used, such as Garford bolt, Durabar bolt, Yielding Secura bolt and Roofex bolt [35,36]. However, most of the experimental studies on the shear performance of bolts still focused on conventional rigid bolts, such as those we described previously. Wu et al. [21] and Chen and Li [26] conducted shear tests and confirmed that energy-absorbing bolts are much better than conventional rigid anchors when passing through a joint surface subjected to pull-shear loading or cyclic shear loading.

Although the fracture mechanisms and anchorage effects of jointed rock masses have been extensively studied considering various joint configurations and anchorage conditions, most of the experimental studies are based on uniaxial or biaxial compression tests. Since the excavation-induced shear slip of joints/fractures is the main cause of rock mass instability, the shear mechanism of the bolted joints/fractures should be studied in depth based on direct shear tests. Although some relevant shear tests have been conducted, as we mentioned earlier, they tend to focus only on continuous planar or rough joints and ignore the discontinuity of joint/fracture structure such as en-echelon fractures. Discontinuous en-echelon fractures have more complex shear behavior than a single continuous fracture due to its complex geometrical structure [6]. However, the shear behavior of bolted en-echelon fractures has never been studied before under direct shear loading. In this study, we innovatively focus on two points: (1) the shear behavior of bolted en-echelon fractures; (2) the quantitative comparison and evaluation on the anchorage effect of energy-absorbing bolt and rigid bolt. This test aims to provide a deeper understanding of the anchorage effect of bolt on en-echelon fractures and to provide valuable suggestions for the design of bolt support for jointed rock masses.

2 Test configuration

2.1 Geometric parameters of en-echelon fractures

To study the shear behavior of bolted en-echelon fractures in the laboratory, an ideal set of en-echelon fractures is first defined, as shown in Fig. 2. The defined en-echelon fractures is composed of several inclined and parallel fracture segments that have a fracture angle i and a fracture length L_j. The rock bridge between two fracture segments has a length of L_r. In addition, the thickness of the fracture zone can be defined as T_j, which can be calculated from the sine of the fracture length, i.e., $T_j=|L_j \cdot \sin i|$. In this research, the fracture angle varies and is defined as positive in counterclockwise and negative in clockwise. Six fracture angles are selected at an interval of 30°, i.e., i=0°, 30°, 60°, 90°, -60° and -30°. The fracture length and rock bridge length remain unchanged at 15 mm and 20 mm, respectively.

2.2 Preparation of bolted specimens

Since it is hard to prefabricate en-echelon fractures in real rock, we use rock-like materials to produce the

specimens. This is widely used in rock mechanics experiments. In this study, the rock-like material is made of plaster, water and retardant in a weight ratio of 1:0.2:0.005 [37], as shown in Fig. 3(a). A metal box with a net volume of 100 mm×100 mm×200 mm was made and a row of metal sheets was inserted., see Fig. 3(b). The mixed slurry was first poured into the metal box and fully shaken to expel the bubbles inside. When it was initially solidified (about 15 minutes), the inserts can be carefully pulled out. After the slurry is completely solidified (about 30 minutes), the sample can be removed from the metal box and cured at room temperature (25°C) for 28 days. It should be noted that each insert is evenly wiped with a layer of lubricant in order to be easily pull out from the sample later, and the prefabricated en-echelon fractures have an initial opening of 1 mm due to the thickness of the inserts. The physical and mechanical properties of rock-like materials at 28 days can be seen in Table 1, which present a good similarity with the properties of sandstone [6].

The installation of bolt was carried out when the specimens were maintained for about 3 days, when it is both easy to drill and reduce impact damage to the specimen. The borehole is 10 mm in diameter, located in the center of the specimen and oriented perpendicular to the fracture zone, see Fig. 3(c). The bolt with a diameter of 6 mm was first placed along the centerline of the borehole, and then grout was injected until the entire borehole was filled, i.e., full-length grouting. The grouting material has the same components as the specimen but in a different ratio of 1:0.32:0.001 [38]. After the grouting material has fully hardened, the pallet and nut can be installed on the exposed end of the bolt, see Fig. 3(d).

2.3 Bolt materials

In this study, two different types of rod materials are chosen to simulate conventional rigid (CR) bolt and energy-absorbing (EA) bolt, as shown in Fig. 4. The tested rigid bolt is a threaded rod made of medium carbon steel (carbon content of 0.25% to 0.45%). Its ultimate tensile strength is about 800 MPa and the yield strength is about 640 MPa. The tested energy-absorbing bolt is an aluminum (Al) alloy material and the main alloying elements are magnesium (Mg, content of 0.8% to 1.2%) and silicon (Si, content of 0.4% to 0.8%). Both types of bolts have a diameter of 6 mm and a length of 105 mm (including the exposed end of 5 mm). The pull-out tests of two types of bolts were performed using an universal testing machines (UH-F1000$_{kN}$XR). The test results show that the two bolts have very different strength and deformation characteristics. At initial loading, both bolts experience a linear elastic stage. Rigid bolt exhibits a tensile stiffness of 4723.4 kN/m, much greater than that of energy-absorbing bolt, i.e., 2924.6 kN/m. Rigid bolt begins to yield when the tensile force reaches 16.7 kN at the tensile displacement of 3.6 mm, and then is followed by a slight hardening phase with the maximum tensile force (19.1kN) at the tensile displacement of 8.3 mm. It was finally pulled-off at about 9.0 mm. Compared to the rigid bolt, energy-absorbing bolt exhibits lower yield force and peak force, i.e., 8.5 kN at the tensile displacement of 3.3 mm and 11.3 kN at 18.3 mm, respectively. However, energy-absorbing bolt exhibits a much larger pull-off displacement of 21.7 mm, meaning an elongation of ~20.7%, approximately 2.4 times that of rigid bolt (~8.6% elongation). In addition, the pull-off pattern of energy-absorbing bolt shows an obvious necking phenomenon (the necking diameter is 3.84 mm, a 36% reduction of the original diameter), which is very slight at the fracture of rigid bolt. The above shows that rigid bolt has a greater strength and stiffness than energy-absorbing bolt, but the later has a greater deformation capacity with a higher elongation and good ductility. The above shows that the two rod materials selected can well simulate the typical mechanical properties of rigid bolt and energy-absorbing bolt and are thus very suitable for laboratory-scale studies.

2.4 Test system and test procedure

Direct shear tests were conducted using a servo-controlled direct shear apparatus [37], as shown in Fig. 5. The shear apparatus can provide normal and shear loads of up to 200 kN by vertical and horizontal jacks. One

linear variable differential transformer (LVDT) is installed in the lower shear box to measure the shear displacement. Four LVDTs are placed at the four corners of the upper shear box to record the vertical displacement. The accuracy of LVDT is 0.001 mm and the range is 0-10 mm. The upper shear box is fixed in the horizontal direction and is subjected to the normal stress applied by the vertical jack. The horizontal jack pushes the lower shear box to move in the shear direction. The LabVIEW-control system can provide an accurate servo-control of boundary conditions e.g., constant normal load (CNL) or constant normal stiffness (CNS). In particular, under CNS conditions, the normal stress changes in time during the shearing process according to the shear-induced dilation or contraction, see Eq.(1) and (2).

$$\Delta\sigma_{\mathrm{n}} = k_{\mathrm{n}} \cdot \Delta\delta_{\mathrm{v}} \tag{1}$$

$$\sigma_{\mathrm{n}}(\mathrm{t}+\Delta\mathrm{t}) = \sigma_{\mathrm{n}}(\mathrm{t}) + \Delta\sigma_{\mathrm{n}} \tag{2}$$

$$k_{\mathrm{n}} = \frac{E}{(1+\nu)} r \tag{3}$$

Where σ_{n} is the normal stress, $\Delta\delta_{\mathrm{v}}$ is the increment of normal displacement, and k_{n} is the normal stiffness. k_{n} is closely related to the deformational properties (elastic modulus E and the Poisson's ratio ν) of rock mass and disturbance scope (or influenced radius r) of underground excavations and can be obtained from expanding the infinite cylinder theory, see Eq.(3) [37, 39].

The bolted specimen is placed into an inner shear box with an elliptical cutting on its upper plate to hold the exposed end of bolt. Then, it is placed into the shear box of shear apparatus and the horizontal and vertical LVDTs are installed. Before shearing, the normal load is applied on the upper shear box at a rate of 0.5 MPa/min to a target value that is the initial normal stress σ_{n0}, set as 1.0 MPa in this test, then the CNS condition is selected (k_{n}=3.0 GPa/m [40]). The shear loading is performed at a constant displacement rate of 0.3 mm/min, and the shear stress, shear displacement and normal displacement are recorded in real time. After the shear test is finished, the postmortem specimen is taken out from the shear box. The failure of en-echelon fractures and bolt are carefully observed and photographed.

3 Test results

3.1 Shear behavior of bolted en-echelon fractures

The test results show that the shearing process of en-echelon fractures involves two stages, the cracking stage (Stage 1) and shear-slip stage (Stage 2), as shown in Fig. 6. Stage 1 mainly involves brittle cracking and coalescence in the rock bridge area, which allows the initial intermittent en-echelon fractures to gradually evolve into a macroscopically through-going shear zone. The shear stress at the cracks coalescence, indicated by a large stress drop, is labeled as SR1 and the corresponding normal dilation is labeled as ND1. With increasing shear displacement, the shear stress grows again to another stress peak (SR2) and then gradually converges to a residual level (SRr), i.e., Stage 2. This stage is characterized by frictional dilation of the through-going shear zone. The dilation and dilation rate at SR2 can be marked as ND2 and v_{d}, respectively and the residual dilation at SRr is marked as NDr.

Fig. 7 shows the curves of shear stress versus shear displacement of en-echelon fractures anchored by two types of bolts. Firstly, we can see that the shear stress curves clearly present a two-stage characteristic, which varies greatly with the fracture angle. At positive angles such as i=0°-60°, see Fig. 7(a)-7(c), the Stage 1 shows a much higher peak stress than that of Stage 2, i.e., SR1>SR2, implying that Stage 1 plays a dominant role in shear resistance although it ends within a small shear displacement. However, as the fracture angle ranges from

positive to negative, see Fig. 7(d)-7(f), Stage 2 gradually rises and becomes the dominant stage, where SR2 is much larger than SR1. Then, it can be noticed that the presence of the bolt does not change the stages of the shearing process, and the demarcation point between the two stages does not change obviously. However, the shear strengths (SR1 and SR2) were improved to varying degrees, depending on the bolt materials and fracture angles. A quantitative analysis can be seen in next section. In addition, we can find that the breakage of bolts usually occurs in Stage 2, which is characterized by an instantaneous drop in shear stress. After the bolt is completely broken, the shear stress decreases to the stress level that would have occurred without bolt. The shear displacement at bolt breakage also varies greatly with the fracture angle and bolt materials. Generally, the breakage of energy-absorbing bolt is much later than that of rigid bolt.

Fig. 8 shows the evolution of normal displacement during the shear of en-echelon fractures. Positive normal displacement represents dilation and the negative represents contraction. We can see that in most cases both shear stages are characterized by dilation. In the case of i=0° and -30°, significant contraction can also be observed in Stage 1. The presence of bolt significantly inhibits the dilation, especially in Stage 2. However, the inhibition effect is quite dependent on the bolt materials and fracture angles. The breakage of the bolt does not cause an instantaneous drop in the normal displacement. Under constant normal stiffness (CNS) conditions, the normal stress varies in line with the normal displacement, as described by Eq.(1) and Eq.(2), see Fig. 9.

3.2 Quantitative evaluation of anchorage effect

Fig. 10 shows a quantitative comparison of the anchoring effect between two types of bolts based on two shear strength indices (SR1 and SR2). From Fig. 10(a), we can see that SR1shows a horizontal S-shaped variation with fracture angle. The maximum value occurs at i=30°, while the minimum value occurs at i=-30°. In general, the presence of bolt promotes a higher SR1, which presents an improvement of 10%-30% in most cases, as shown in Fig. 10(c). And, rigid bolt shows a better reinforcement effect than energy-absorbing bolt. For example, at i=-30°, SR1 shows an improvement of nearly 50% by rigid bolt. In previous section, we know that the cracking stage (Stage 1) usually occurs within a very small shear displacement (usually less than 1.0 mm). In fact, such a small shear deformation will not largely motivate the shear resistance of the bolt. The improvement in SR1 is mainly attributed to the increase in shear stiffness of rock mass by bolting. Since rigid bolt has a greater shear stiffness than energy-absorbing bolt, it exhibits a better reinforcement effect on SR1.

Fig. 10(b) and 10(d) show the anchorage effect of bolt on SR2. In Fig. 10(b), SR2 presents an asymmetric V-shaped variation with the fracture angle. The SR2 at a negative angle (e.g., i=-60°) is always greater than that at the corresponding positive angle (e.g., i=60°). This is caused by the different shear failure structures at different fracture angles (Section 3.3). Two types of bolts produce different degrees of reinforcement effect on SR2, and both show the maximum reinforcement when i=0°, i.e., 64.7% (rigid bolt) and 41.8% (energy-absorbing bolt), respectively, see Fig. 10(d). At negative fracture angles, the reinforcement by rigid bolt is much greater (about 1.8-2.4 times) than that of energy-absorbing bolt. For example, at i=-30°, rigid bolt produces a 32.0% reinforcement, while energy-absorbing bolt has only 17.1%. However, at positive fracture angles, energy-absorbing bolt shows a greater reinforcement on SR2 than rigid bolt. For example, at i=30° and i=60°, the reinforcement by energy-absorbing bolt is about 1.57 and 1.61 times that of rigid bolt, respectively. The above shows that the two types of bolts have significantly different bolting performance on SR2 and this depends greatly on the fracture angle. This phenomenon is essentially determined by the interaction between the bolt and the shear failure structures of en-echelon fractures, which will be discussed in Section 4.

Fig. 11 further shows the anchoring effect of two types of bolts on four dilation indices (ND1, ND2, v_d and NDr). In Fig. 11(a), ND1 exhibits a near V-shaped variation with the fracture angle. The minimum value occurs at i=-30°, meaning a tiny dilation such as 0.028 mm under no bolt or even a contraction such as -0.215 mm in

the case of rigid bolt. At positive fracture angles, such as i=30°~90°, ND1 exhibits a large dilation of 0.4-0.6 mm, where the effect of the bolt is relatively small. In Fig. 11(b), ND2 exhibits large dilation except for the case of i=0°. The bolt has a noticeable dilation-inhibiting effect on ND2, which is highly dependent on the fracture angle and bolt materials. At positive fracture angles, rigid bolt has a greater dilation-inhibiting effect than energy-absorbing bolt. For example, at i=30° and i=60°, ND2 is reduced by 47.8% and 35.3% by rigid bolt, respectively, which are much greater than 29.1% and 13.9% by energy-absorbing bolt. However, the opposite is true at negative fracture angles, a lower ND2 is produced by energy-absorbing bolt, with a reduction of 19.1% and 28.3% at i=-30° and i=-60°, respectively. The difference in the dilation-inhibiting effect between the two types of bolts is mainly caused by the different bolt deformation mechanisms, which are also closely related to the shear failure structures (Section 4).

Comparing Fig. 11(b) and 11(c), we can find that the peak dilation rate v_d varies quite differently from the ND2. In Fig. 11(c), the v_d at a negative angle is much larger than that at a positive angle. For example, in the case of no bolt, v_d at i=-30° and -60° is 0.34 and 0.27 respectively, corresponding to the dilation angle of 19.1° and 15.3°. However, at i=30° and 60°, v_d is 0.11 and 0.12 respectively, corresponding to the dilation angle of 6.4° and 6.8°. The difference in dilation rate (or dilation angle) directly reflects the difference in morphology of shear failure structures (Section 3.3). The effect of energy-absorbing bolt on the peak dilation rate v_d is not as pronounced as on the peak dilation ND2. Only a decrease of less than 10% in v_d can be produced by energy-absorbing bolt. However, rigid bolt shows a great influence on v_d. At positive fracture angles, a significant reduction, such as 61.1% at i=30° and 33.1% at i=60°, can be produced by rigid bolt, implying a strong inhibiting effect on peak dilation rate. Whereas, at negative fracture angles, especially at i=-30°, rigid bolt contributes a large increase of 38.8% in v_d, although here it still shows an inhibition on peak dilation ND2. In Fig. 11(d), the final dilation NDr presents a similar variation to the peak dilation ND2, but the dilation-inhibiting effect of bolt on NDr is more pronounced, especially at negative fracture angles. For example, at i=-60°, NDr is largely reduced by 67.4% (energy-absorbing bolt) and 42.2% (rigid bolt), respectively. Both Fig. 11(b) and 11(d) illustrate that in terms of dilation-inhibiting effect, rigid bolt behaves better than energy-absorbing bolt at positive fracture angles, while the opposite is true at negative fracture angles.

3.3 Shear failure and bolt breakage

As shown in Section 3.1 and 3.2, the anchorage effect of bolt on shear strength and dilation of en-echelon fractures is highly dependent on the fracture angle. This is because different fracture angles will produce different shear failure structures, which further affect the bolt deformation characteristics. In this section, three typical shear failure structures can be summarized as planar failure structure, sawtooth failure structure and block failure structure, as shown in Fig. 12.

(1) Planar failure structure, see Fig. 12(a). It occurs only at i=0°. The coalescence of the rock bridge is dominated by a mixed cracking in tensile and shear. The shear crack first initiates at the fracture tip and extends for a short distance along a small inclination to the shear direction. Then, the two shear cracks are connected by an extension crack. As the shear displacement increases, the extension segment shows an obvious openness. Planar failure structure tends to have a lower shear strength (e.g., SR2, Fig. 10(b)) and dilation (e.g., ND2, Fig. 11(b)), but can fully exert the shear resistance of bolts in Stage 2, as shown in Fig. 10(d).

(2) Sawtooth failure structure, see Fig. 12(b). It occurs at negative fracture angles, e.g., i=-30° and -60°. The cracking of rock bridge is mainly dominated by wing crack, which initiates at the fracture tip and propagate to the nearer tip of the adjacent fracture, finally cutting out an subelliptical block in the bridge area. With increasing shear displacement, these blocks are gradually crushed by the rock walls, forming obvious pull-aparts zones. Caused by the sawtooth climbing during shear, sawtooth failure structure usually has a larger dilation rate (or

dilation angle, Fig. 11(c)) and thus a larger shear strength SR2 (Fig. 10(b)). From the perspective of strength reinforcement, rigid bolt has a better anchoring effect on sawtooth failure structures than energy-absorbing bolt, while its dilation-inhibiting effect is inferior to the latter.

(3) Block failure structure, see Fig. 12(c). It occurs at positive fracture angles, e.g., i=30°~90°. The cracking of rock bridges is governed by wing crack and shear crack. Wing crack initiates at the fracture tip and propagates to the more distant tip of adjacent fracture, and then interconnects through a short shear crack. As a result, the bridge region is cut out as a parallelogram-like block. With increasing shear displacement, block rotation and shear-slip on the block surface (precisely, where the shear cracks are located) dominate the Stage 2. Compared to sawtooth failure structure, block failure structure produces a much lower dilation rate (or dilation angle, Fig. 11(c)) and thus a lower shear strength (SR2, Fig. 10(b)). Energy-absorbing bolt is more favorable to improve the shear strength of block failure structure than rigid bolt, but the latter has a better dilation-inhibiting effect.

Fig. 13 further shows the morphological characteristics of the three shear failure structures, as well as the deformation and failure of the two bolts. In sawtooth failure structure, see Fig. 13(a) and 13(b), the blocks are finally crushed and broken into fine gouges set between the sawtooths. Obvious traces of slippage and shearing-off on the sawtooths can be observed. In block failure structure, see Fig. 13(c) and 13(d), strips of slip traces can be clearly observed on the block surface. However, in planar failure structure, see Fig. 13(e) and Fig. 13(f), only slight slip traces can be observed on the flat fracture surface. After shearing, rigid bolts usually break into three segments and the intermediate segment through the shear zone can be directly observed. The length of the intermediate segment varies with the shear failure structure, which will be discussed in Section 4.2. Near the fracture of rigid bolt, a wedge-shaped damage area is often observed, caused by the squeezing between the bolt and the hole wall. However, energy-absorbing bolt usually breaks into two sections with significant necking and bending near the fracture. The above shows that rigid bolt and energy-absorbing bolt present completely different deformation and breakage characteristics.

4 Discussion

4.1 Deformation mechanism of bolt

There is a close interaction between shear failure structure and bolt deformation, which can be depicted in Fig. 14. In the block failure structure, the block rotation will cause a significant dilation and this imposes an axial tensile force (F_t) on the bolt, see Fig. 14(a). For energy-absorbing bolt, its low tensile stiffness allows a large bolt elongation and thus a large dilation of shear zone, such as $\Delta\delta_v^A$. However, the rigid bolt with a high tensile stiffness will greatly inhibit the increase in dilation and thus results in a smaller dilation $\Delta\delta_v^B$ than $\Delta\delta_v^A$. This explains why the ND2 with energy-absorbing bolt is greater than that with rigid bolt at i=30° and 60° in Fig. 11(b). More importantly, a larger dilation will induce a higher normal stress under CNS conditions, which is the main reason for a higher SR2 of block failure structure anchored by energy-absorbing bolt.

In the sawtooth failure structure, the bolt directly passes through the sawtooth surface. Thus, sawtooth climbing during shearing will cause a direct shear force (F_s) on the bolt near the interface, as shown in Fig. 14(b). For energy-absorbing bolt, its good ductility allows the deformed section to present a larger dip angle α_A, which consequently produces a smaller dilation increment $\Delta\delta_v^A$. However, the deformed section of rigid bolt exhibits a smaller dip angle α_B and thus a larger dilation increment $\Delta\delta_v^B$ than $\Delta\delta_v^A$. This explains why the ND2 with rigid bolt is larger than that with energy-absorbing bolt at i=-30° and -60° in Fig. 11(b). The above implies that a higher SR2 of sawtooth failure structure with rigid bolt is mainly attributed to two aspects: (1) The shear resistance of the rigid bolt can be fully motivated under direct shear force; (2) The small deformation of the rigid bolt promotes a larger dilation and thus a higher normal stress under CNS conditions.

4.2 Breakage displacement of bolt

The shear displacement at bolt breakage (referred to as breakage displacement, δ_h^b) is another important parameter of interest, as it determines how long the anchoring effect of the bolt can last. Previously, we have seen in Fig. 7 that the breakage displacement of bolt highly depends on the bolt material and the fracture angle. Fig. 15 shows quantitatively the variation of breakage displacement, which presents an approximate V-shape for both types of bolts. The δ_h^b usually has a minimum value at i=0° and a maximum value at i=90°. And, the difference of δ_h^b between a pair of positive and negative angles (e.g., i=60° & -60°) is not significant. Generally, the δ_h^b of energy-absorbing bolt is more than two times that of rigid bolt. Fig. 15(a) enlightens us that for the same type of bolt, δ_h^b is only related to the absolute value of the fracture angle (i), which essentially reflects the thickness (T_j) of the en-echelon fracture zone at a certain fracture length (L_j), i.e., $T_j=|L_j \cdot \sin i|$, as shown in Fig. 2.

To better predict the breakage displacement of bolt, we prefer a dimensionless treatment. For example, δ_h^b can be dimensionless by dividing by the bolt diameter (D_b), i.e., δ_h^b/D_b, and L_j can be dimensionless by dividing by the rock bridge length (L_r), i.e., $k_j=L_j/L_r$. The k_j can also be interpreted as an index characterizing the persistency of the en-echelon fractures. Thus, the relationship between δ_h^b and i can be redescribed with $k_j \cdot \sin i$ as the horizontal coordinate and δ_h^b/D_b as the vertical coordinate, as shown in Fig. 15(b), where a quadratic relationship can be observed. In particular, the energy-absorbing bolt shows a high degree of fitting. The different fit coefficients between the two bolts, such as the second-order coefficient (energy-absorbing bolt:1.02, rigid bolt: 0.45), precisely reflect the differences in the deformation properties of the bolts. Therefore, an equation can be proposed to predict the breakage displacement of bolts, see Eq.(4).

$$\delta_h^b / D_b = f_p (k_j \cdot \sin i)^2 + C_0 \tag{4}$$

Where, f_p can be interpreted as the deformation factor of the bolt. C_0 can be determined by the breakage displacement of the bolt at i=0°.

In this research, the deformation factor f_p of the bolt is found to be related to the length of the deformed section of the bolt crossing the fracture zone and can be defined by a ratio, i.e., $f_p= L_{MN}/L_{PQ}$, as shown in Fig. 16. L_{MN} measures the length of an ideal deformation segment by considering fracture zone thickness (T_j) and shear displacement ($\Delta\delta_h$), i.e., $L_{MN}^2=\Delta\delta_h^2+T_j^2$. The dilation value ($\Delta\delta_v$) is not considered because it is very small (usually less than 1.0 mm) compared to the fracture zone thickness and is difficult to estimate. L_{PQ} measures the actual length of the deformed section of the bolt, which can be determined by the distance between two plastic points (P and Q). Due to a larger shear stiffness, the rigid bolt usually shows a larger L_{PQ} than that of energy-absorbing bolt and thus has a smaller deformation factor.

Fig. 17 presents the failed bolts removed from the postmortem specimens, which allow us to directly measure the L_{PQ} value of the bolts. For rigid bolts in Fig. 17(a), L_{PQ} is the length of the intermediate section of the broken bolt. For energy-absorbing bolts in Fig. 17(b), L_{PQ} is the length of the yielding section between two plastic points (where significant bending of the bolt begins to occur). Based on the known breakage displacement (δ_h^b) and L_{PQ} value, the deformation factor f_p of bolts can be calculated in each case, see Table 2. From Fig. 18(a) we can see that f_p is little influenced by the fracture angle i and depends mainly on the bolt material. The energy-absorbing bolt and rigid bolt show an average deformation factor of 0.92 and 0.57, respectively, which are very close to the second-order coefficients (1.02 and 0.45) of the fitted curves in Fig. 15(b). When we use the measured f_p to predict the δ_h^b according to Eq.(4), a good agreement was observed between the test and predicted values, as shown in Fig. 18(b) And, the prediction error is acceptable, an average error is 2.96% for energy-absorbing bolt and 5.45% for rigid bolt, see Table 3.

As mentioned earlier, C_0 in Eq.(4) can be determined by the δ_h^b at i=0°. In the laboratory, we can conduct a direct shear test of a through-going planar joint anchored by a bolt to approximately obtain the δ_h^b and L_{PQ} value at i=0°, for example, denoted as δ_{h0}^b and L_{PQ0}. Then, $C_0=\delta_{h0}^b/D_b$ and $f_p=\delta_{h0}^b/L_{PQ0}$. However, this method is better suited for the case of a large joint persistency, such as k_j=0.75 for this research or larger. This is because, a high persistency at i=0° corresponds to a nearly planar failure structure (Fig. 12(a)), while with decreasing persistency, e.g., k_j<0.5, the typical failure structures shown in Fig. 12 will degenerate into irregular failure structures [6], where the irregular roughness becomes the main factor affecting the deformation and breakage of bolts.

4.3 Evaluation of bolt contribution

In many cases, such as i=0°, -30°, -60° and 90°, the rigid bolt promotes a larger shear strength, while its breakage displacement is much smaller than that of energy-absorbing bolt. In field, it may be unreasonable to evaluate the anchorage effect of the bolt based only on shear strength or breakage displacement. Here, we propose a bolt contribution index C_b to evaluate the bolting performance comprehensively considering both the shear strength and breakage displacement, as shown in Fig. 19(a). The bolt contribution index can be calculated according to Eq.(5).

$$C_b = (W_b - W_n) / W_n \times 100\% \tag{5}$$

Where, W_b is the area enclosed by the shear stress curve with bolting in the range of shear displacement from δ_h^1 to δ_h^b, and W_n is the area without bolting. W_b-W_n is considered as the bolt contribution value. We should state that the calculation of bolt contribution is mainly considered in Stage 2, since the cracking stage (Stage 1) usually ends within a very small shear displacement.

Fig. 19(b) shows a comparison of the contribution index C_b between the two types of bolts at various fracture angles. We can see that at positive fracture angles, energy-absorbing bolt exhibits a greater contribution than rigid bolt. In particular, when i=30° and 60°, the C_b of energy-absorbing bolt is nearly 2-3 times higher than that of rigid bolt. However, when the fracture angle is negative, energy-absorbing bolt tends to be less advantageous. In particular, at i=-30°, the C_b of rigid bolt reaches 1.8 times that of energy-absorbing bolt. The above implies that in the bolt support design for rock engineerings involving en-echelon fractures, the geometrical factor such as the fracture angle should be taken into account for a more rational and economical selection of bolt types. In general, energy-absorbing bolt is optimal in conditions where block failure structures may occur, while in conditions dominated by planar or sawtooth failure structures, conventional rigid bolt can be selected.

5 Conclusions

In this study, the anchorage effect of bolt on en-echelon fractures is investigated based on direct shear tests. Two types of bolts, i.e., energy-absorbing (EA) bolt and conventional rigid (CR) bolt are focused and compared. The shear failure structures of en-echelon fractures as well as the bolt deformation mechanisms are analyzed. The prediction of breakage displacement of bolt and the evaluation of bolt contribution are also discussed. The main conclusions drawn are as follows.

(1) The shear process of en-echelon fractures involves two stages: the cracking stage (Stage 1) and the shear-slip stage (Stage 2). They can be characterized by two shear strength indices and four dilation indices. The presence of bolt will not change the stages of the shear process, but can affect the shear strength and dilation to varying degrees.

(2) Bolts can improve the shear strength of the en-echelon fractures, while the reinforcement effect is closely

related to the bolt material and fracture angle. Rigid bolt usually shows a better reinforcement on the cracking strength SR1 than energy-absorbing bolt at various fracture angles. However, for shear strength SR2, rigid bolt performs better only at negative fracture angles.

(3) Both types of bolts have a significant dilation-inhibiting effect especially in Stage 2. When the fracture angle is positive, rigid bolt shows a greater inhibition effect than energy-absorbing bolt, while the opposite is true at negative fracture angles. In addition, rigid bolt also greatly affects the peak dilation rate of Stage 2, which is reduced at positive fracture angles, however is increased at negative fracture angles.

(4) En-echelon fractures present three different shear failure structures, which are responsible for the different bolt deformation mechanisms. In block failure structures, energy-absorbing bolt can better release the dilation caused by block rotation due to a lower deformation stiffness of bolt, thus promoting a higher normal stress and shear strength under constant normal stiffness conditions. In sawtooth failure structures, the shear resistance of rigid bolt can be better activated by the direct shear forces caused by sawtooth climbing.

(5) A deformation factor can be used to characterize the deformation properties of the bolt and to predict the breakage displacement of the bolt. In addition, a bolt contribution index is proposed to evaluate the bolting performance comprehensively considering shear strength and breakage displacement. In general, energy-absorbing bolt is optimal in conditions where block failure structures occur. However, in conditions dominated by planar or sawtooth failure structures, conventional rigid bolt can be selected.

Conflict of interest

The authors declare that they have no conflicts of interest.

Acknowledgements

This research was supported by National Natural Science Foundation of China (52004145), Natural Science Foundation of Shandong Province (ZR2020QE119) and China Scholarship Council (CSC.201806420027).

References

[1] E. Lajtai, B. Carter, E. Duncan, En echelon crack-arrays in potash salt rock, Rock Mech. Rock Eng. 27 (1994) 89-111.

[2] A.G. McGrath, I. Davison, Damage zone geometry around fault tips, Journal of Structural Geology 17 (1995) 1011-1024.

[3] M.A. Brideau, M. Yan, D. Stead, The role of tectonic damage and brittle rock fracture in the development of large rock slope failures, Geomorphology 103 (2009) 30-49.

[4] D. Huang, D. Cen, G. Ma, R. Huang, Step-path failure of rock slopes with intermittent joints, Landslides 12 (2015) 911-926.

[5] Y. Cheng, L.N.Y. Wong, C. Zou, Experimental study on the formation of faults from en-echelon fractures in Carrara Marble, Engineering Geology 195 (2015) 312-326.

[6] Y. Zhang, Y. Jiang, D. Asahina, Z. Wang, Structural effect of en-echelon fractures on shear behavior of rock mass under constant normal load conditions: an experimental study, Rock Mech. Rock Eng. 54 (2021) 4825–4849.

[7] D.C.P. Peacock, M.W. Anderson, The scaling of pull-aparts and implications for fluid flow in areas with strike-slip faults, Journal of Petroleum Geology 35 (2012) 389-399.

[8] D.C.P. Peacock, D.J. Sanderson, Pull-aparts, shear fractures and pressure solution, Tectonophysics 241 (1995) 1-13.

[9] Y.S. Kim, D.C.P. Peacock, D.J. Sanderson, Mesoscale strike-slip faults and damage zones at Marsalforn,

Gozo Island, Malta, Journal of Structural Geology 25 (2003) 793-812.
[10] Y.S. Kim, D.C.P. Peacock, D.J. Sanderson, Fault damage zones, Journal of Structural Geology 26 (2004) 503-517.
[11] G. Grasselli, 3D behaviour of bolted rock joints: experimental and numerical study, International journal of rock mechanics and mining sciences 42 (2005) 13-24.
[12] L.P. Srivastava, M. Singh, Effect of fully grouted passive bolts on joint shear strength parameters in a blocky mass, Rock Mech. Rock Eng. 48 (2015) 1197-1206.
[13] H. Kang, J. Li, J. Yang, Gao, F. Investigation on the influence of abutment pressure on the stability of rock bolt reinforced roof strata through physical and numerical modeling, Rock Mech. Rock Eng. 50 (2017) 387-401.
[14] H.W. Jing, S.Q. Yang, M.L. Zhang, G.A. Xu, K.F. Chen, An experimental study on anchorage strength and deformation behavior of large-scale jointed rock mass, Tunnelling and Underground Space Technology 43 (2014) 184-197.
[15] Y. Li, C. Li, L. Zhang, W. Zhu, S. Li, J. Liu, An experimental investigation on mechanical property and anchorage effect of bolted jointed rock mass, Geosciences Journal 21 (2017) 253-265.
[16] B. Meng, H. Jing, S. Yang, Y. Wang, B. Li, Experimental study on the shear behavior of bolted concrete blocks with oblique shear test, Advances in Civil Engineering (2018) 7281218.
[17] H. Jalalifar, N. Aziz, Experimental and 3D numerical simulation of reinforced shear joints, Rock Mech. Rock Eng. 43 (2010) 95-103.
[18] Q. Wang, R. Pan, S.C. Li, H.T. Wang, B. Jiang, The control effect of surrounding rock with different combinations of the bolt anchoring lengths and pre-tightening forces in underground engineering, Environmental Earth Sciences 77 (2018) 1-14.
[19] S.Q. Yang, M. Chen, Y.H. Huang, H.W. Jing, P.G. Ranjith, An experimental study on fracture evolution mechanism of a non-persistent jointed rock mass with various anchorage effects by DSCM, AE and X-ray CT observations, International Journal of Rock Mechanics and Mining Sciences 134 (2020) 104469.
[20] G. Wang, Y. Zhang, Y. Jiang, P. Liu, Y. Guo, J. Liu, S. Wang, Shear behaviour and acoustic emission characteristics of bolted rock joints with different roughnesses, Rock Mechanics and Rock Engineering 51 (2018) 1885-1906.
[21] X. Wu, Y. Jiang, B. Gong, T. Deng, Z. Guan, Behaviour of rock joint reinforced by energy-absorbing rock bolt under cyclic shear loading condition, Int J Rock Mech Min Sci 110 (2018) 88-96.
[22] X. Wu, Y. Jiang, B. Gong, Z. Guan, T. Deng, Shear performance of rock joint reinforced by fully encapsulated rock bolt under cyclic loading condition, Rock Mechanics and Rock Engineering 52 (2019) 2681-2690.
[23] K. Skrzypkowski, Case studies of rock bolt support loads and rock mass monitoring for the room and pillar method in the Legnica-Głogów Copper District in Poland, Energies 13 (2020) 2998.
[24] K. Skrzypkowski, W. Korzeniowski, K. Zagórski, A. Zagórska, Modified rock bolt support for mining method with controlled roof bending, Energies 13 (2020) 1868.
[25] A. Ferrero, The shear strength of reinforced rock joints, International journal of rock mechanics and mining sciences & geomechanics abstracts 32 (1995) 595-605.
[26] Y. Chen, C.C. Li, Performance of fully encapsulated rebar bolts and D-bolts under combined pull-and-shear loading, Tunnelling and Underground Space Technology 45 (2015) 99-106.
[27] X. Li, N. Aziz, A. Mirzaghorbanali, J. Nemcik, Behavior of fiber glass bolts, rock bolts and cable bolts in shear, Rock Mech. Rock Eng. 49 (2016) 2723-2735.
[28] H. Jalalifar, N. Aziz, M. Hadi, The effect of surface profile, rock strength and pretension load on bending

behaviour of fully grouted bolts, Geotechnical & Geological Engineering 24 (2006) 1203-1227.
[29] K. Spang, P. Egger, Action of fully-grouted bolts in jointed rock and factors of influence, Rock Mech. Rock Eng. 23 (1990) 201-229.
[30] M. He, W. Gong, J. Wang, P. Qi, Z. Tao, S. Du, Y. Peng, Development of a novel energy-absorbing bolt with extraordinarily large elongation and constant resistance, International Journal of Rock Mechanics and Mining Sciences 67 (2014) 29-42.
[31] M. He, C. Li, W. Gong, L.R. Sousa, S. Li, Dynamic tests for a Constant-Resistance-Large-Deformation bolt using a modified SHTB system, Tunnelling and Underground Space Technology 64 (2017) 103-116.
[32] D.R. Mccreath, P.K. Kaiser, Current support practices in burst-prone ground, mining research directorate. Sudbury:Laurentian University, 1995.
[33] A. Anders, Laboratory testing of a new type of energy absorbing rock bolt, Tunnelling and Underground Space Technology 20 (2005) 291-330.
[34] C.C. Li, A new energy-absorbing bolt for rock support in high stress rock masses, International Journal of Rock Mechanics and Mining Sciences 47 (2010) 396-404.
[35] F. Charette, M. Plouffe, A new rock bolt concept for underground excavations under high stress conditions, In Proceedings of 6th International Symposium on Ground Support in Mining and Civil Engineering Construction, Johannesburg (2008) 225-240.
[36] M.C. He, Z.B. Guo, Mechanical property and engineering application of anchor bolt with constant resistance and large deformation, Chinese Journal of Rock Mechanics and Engineering 33 (2014) 1297-1308.
[37] Y. Jiang, J. Xiao, Y. Tanabashi, T. Mizokami, Development of an automated servo-controlled direct shear apparatus applying a constant normal stiffness condition, International Journal of Rock Mechanics and Mining Sciences 41 (2004) 275-286.
[38] Y. Zhang, Y. Jiang, C. Wang, M. Chen, Q. Yin, Shear of bolted non-persistent joints: role of bolting conditions and joint persistency, Géotechnique Letters 10 (2020) 550-558.
[39] I.W. Johnston, T.S.K. Lam, A.F. Williams, Constant normal stiffness direct shear testing for socketed pile design in weak rock, Geotechnique 37 (B1) (1987) 83-87.
[40] Y. Zhang, Y. Jiang, D. Asahina, Z. Wang, Shear behavior and acoustic emission characteristics of en-echelon joints under constant normal stiffness conditions, Theoretical and Applied Fracture Mechanics 109 (2020) 102772.

(a) Step-path failure caused by en-echelon fractures [3,4].

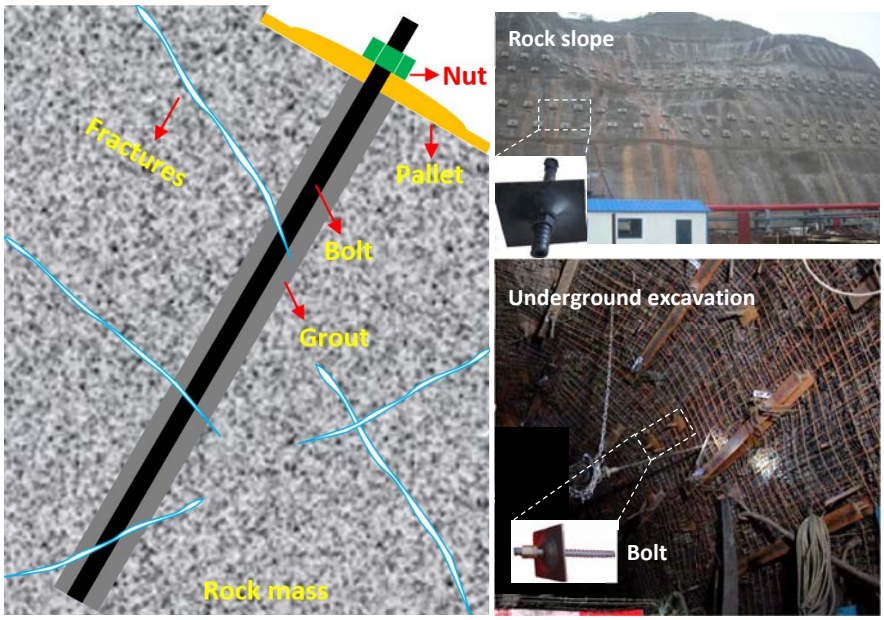

(b) Bolt support in jointed rock mass

Fig.1 En-echelon fractures in natural rock mass and bolt support in rock engineerings.

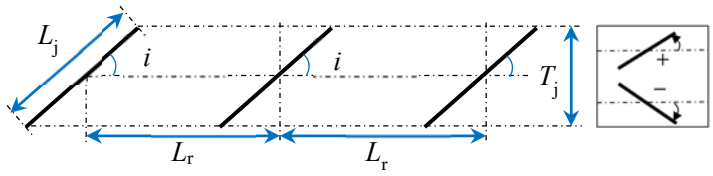

i-Fracture angle L_r-Length of rock bridge

L_j-Length of each fracture T_j-Thickness of fracture zone

Fig. 2. Schematic diagram of en-echelon fractures and defined structural parameters

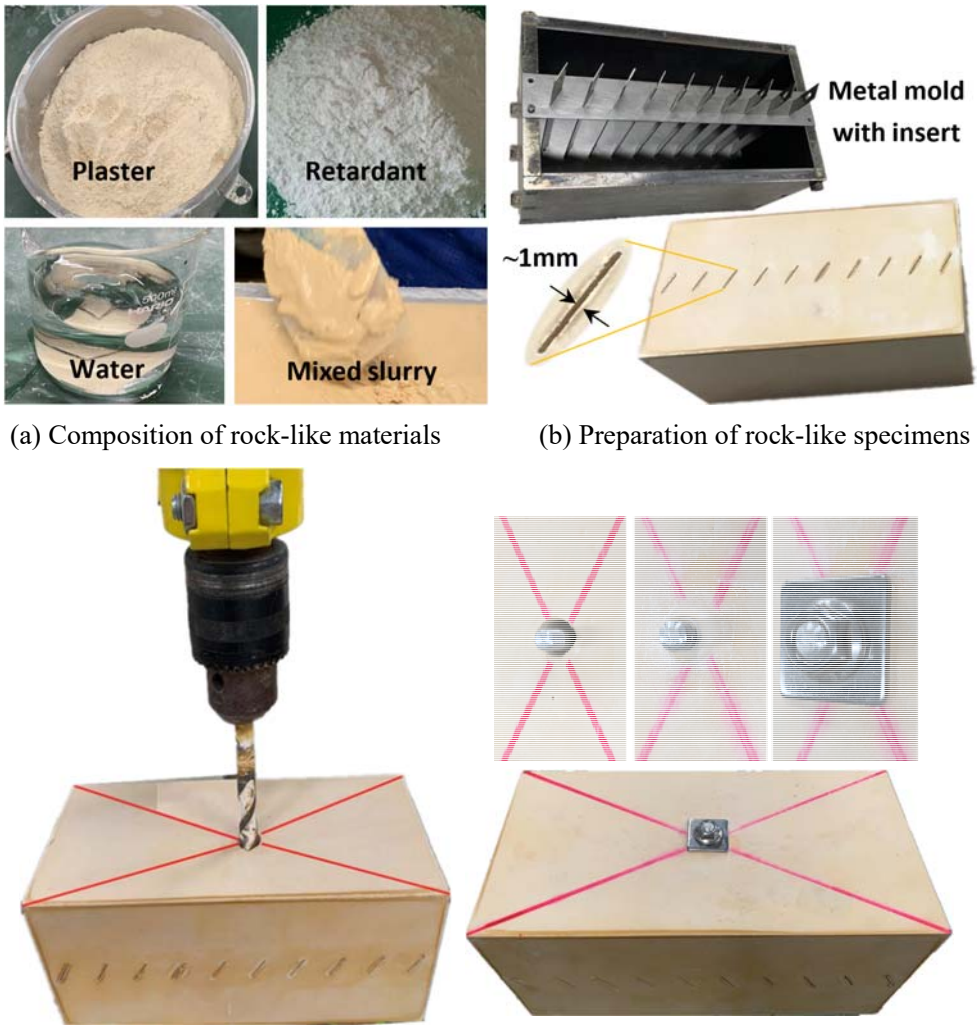

(a) Composition of rock-like materials (b) Preparation of rock-like specimens

(c) Drill a through hole (d) Installation of bolt

Fig. 3 Sample preparation, test system and test procedure

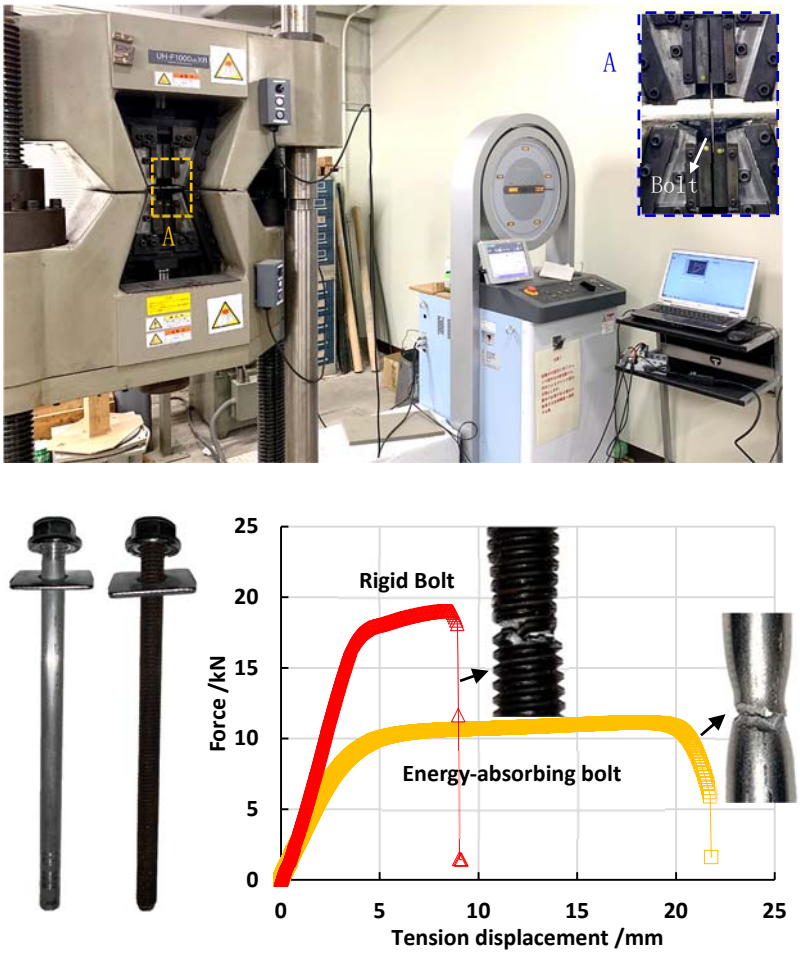

Fig.4 Mechanical testing of bolt materials.

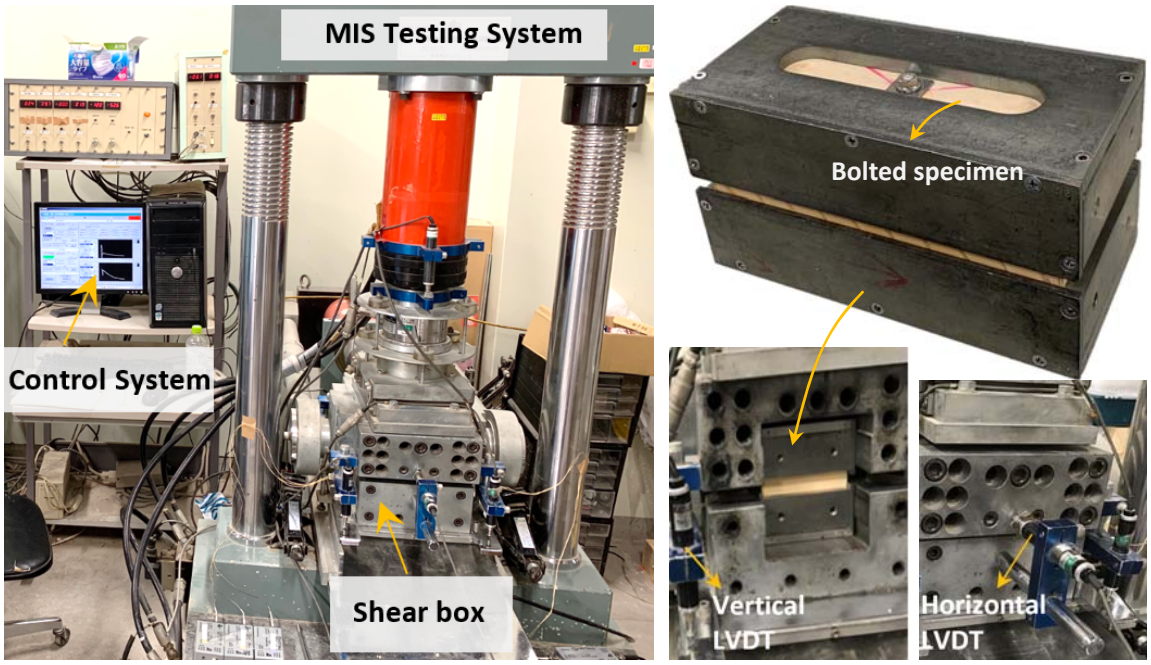

Fig.5 Test system and test procedure.

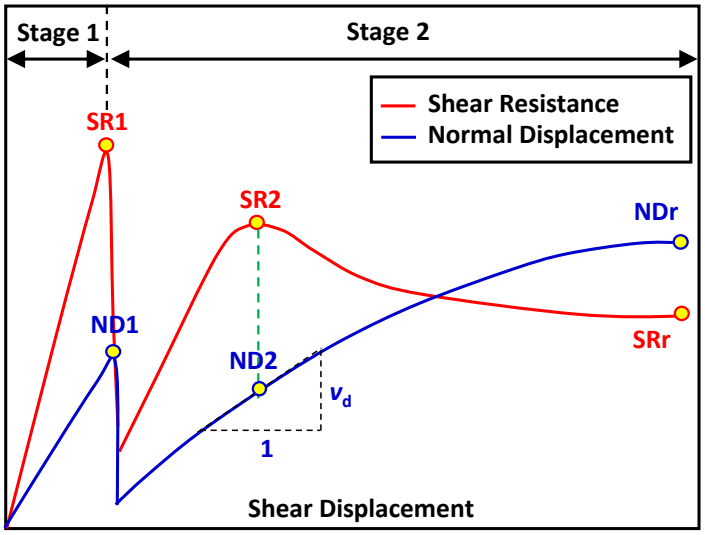

Fig.6 A typical shear response of en-echelon fractures

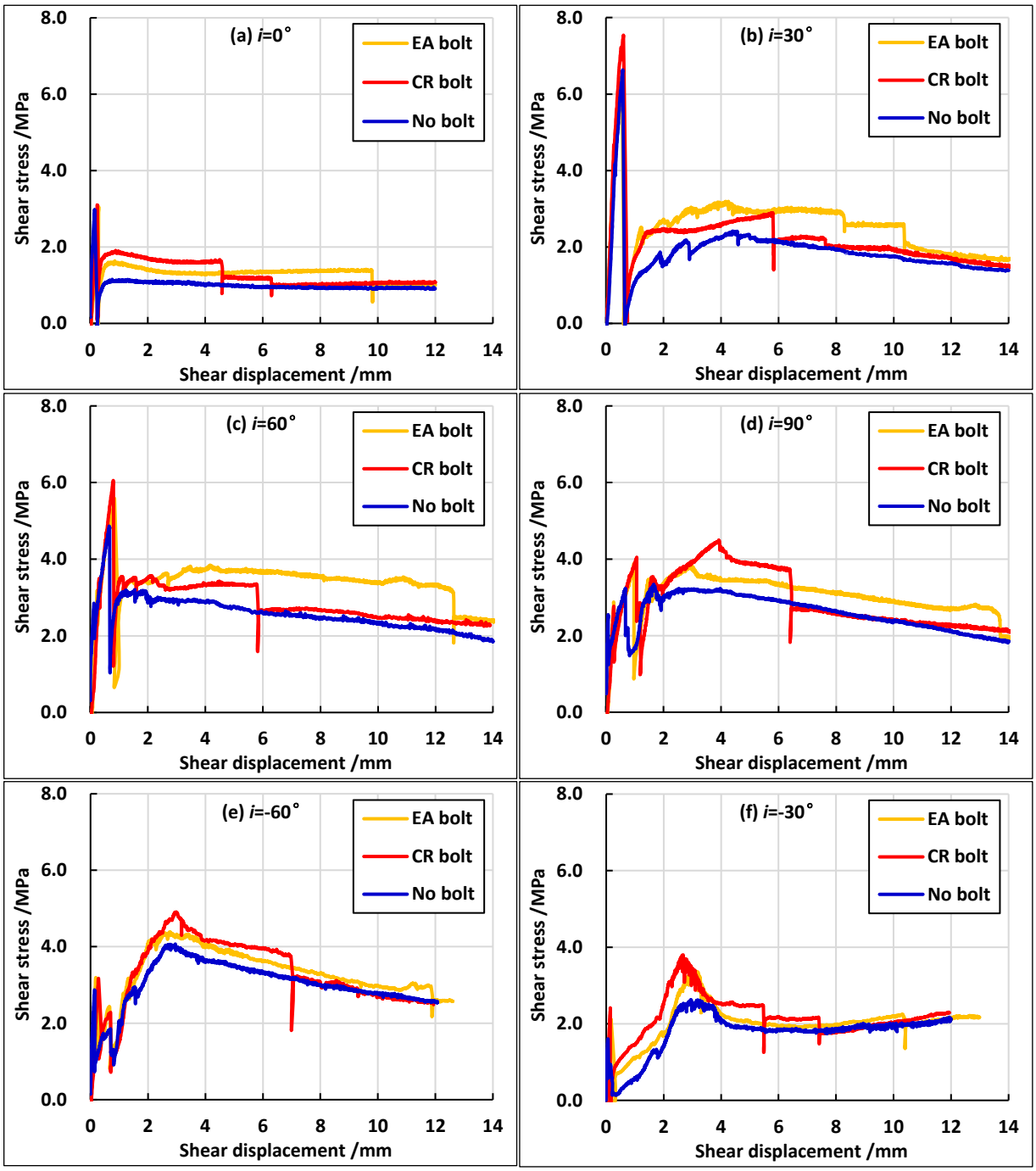

Fig. 7 Curves of shear stress versus shear displacement of bolted en-echelon fractures (EA bolt: energy-absorbing bolt, CR bolt: conventional rigid bolt)

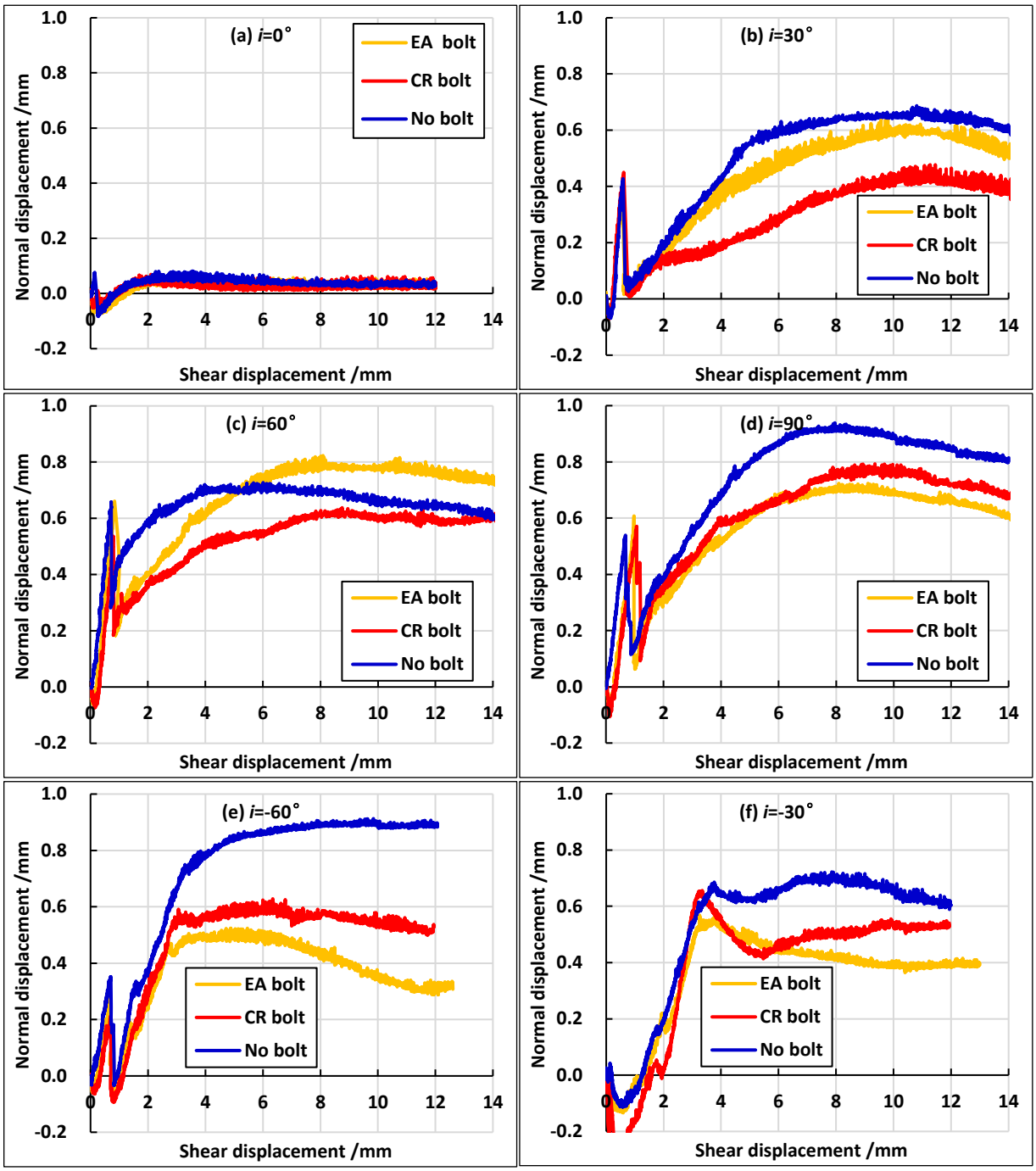

Fig. 8 Curves of normal displacement versus shear displacement of bolted en-echelon fractures (EA bolt: energy-absorbing bolt, CR bolt: conventional rigid bolt)

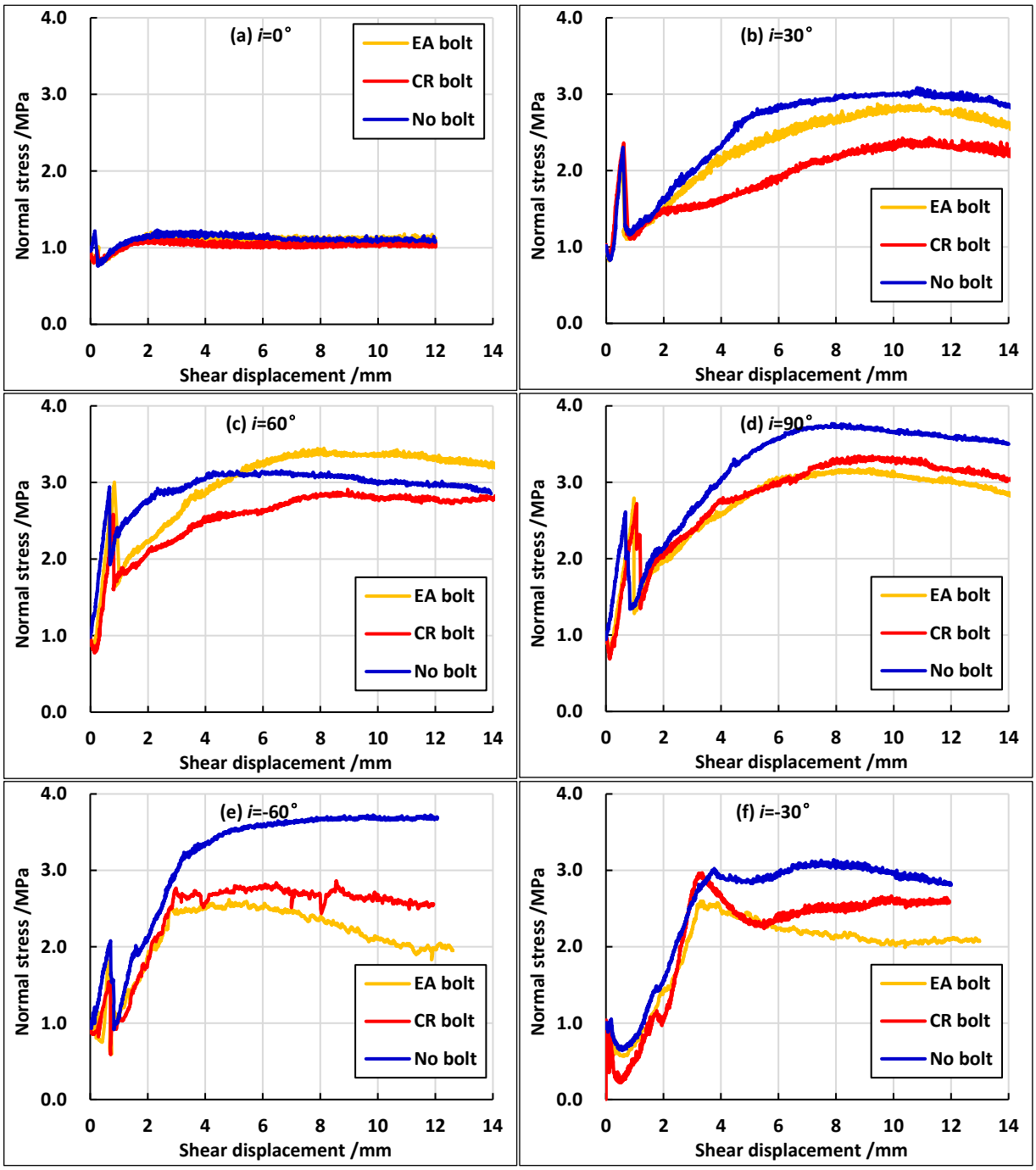

Fig. 9 Curves of normal stress versus shear displacement of bolted en-echelon fractures (EA bolt: energy-absorbing bolt, CR bolt: conventional rigid bolt)

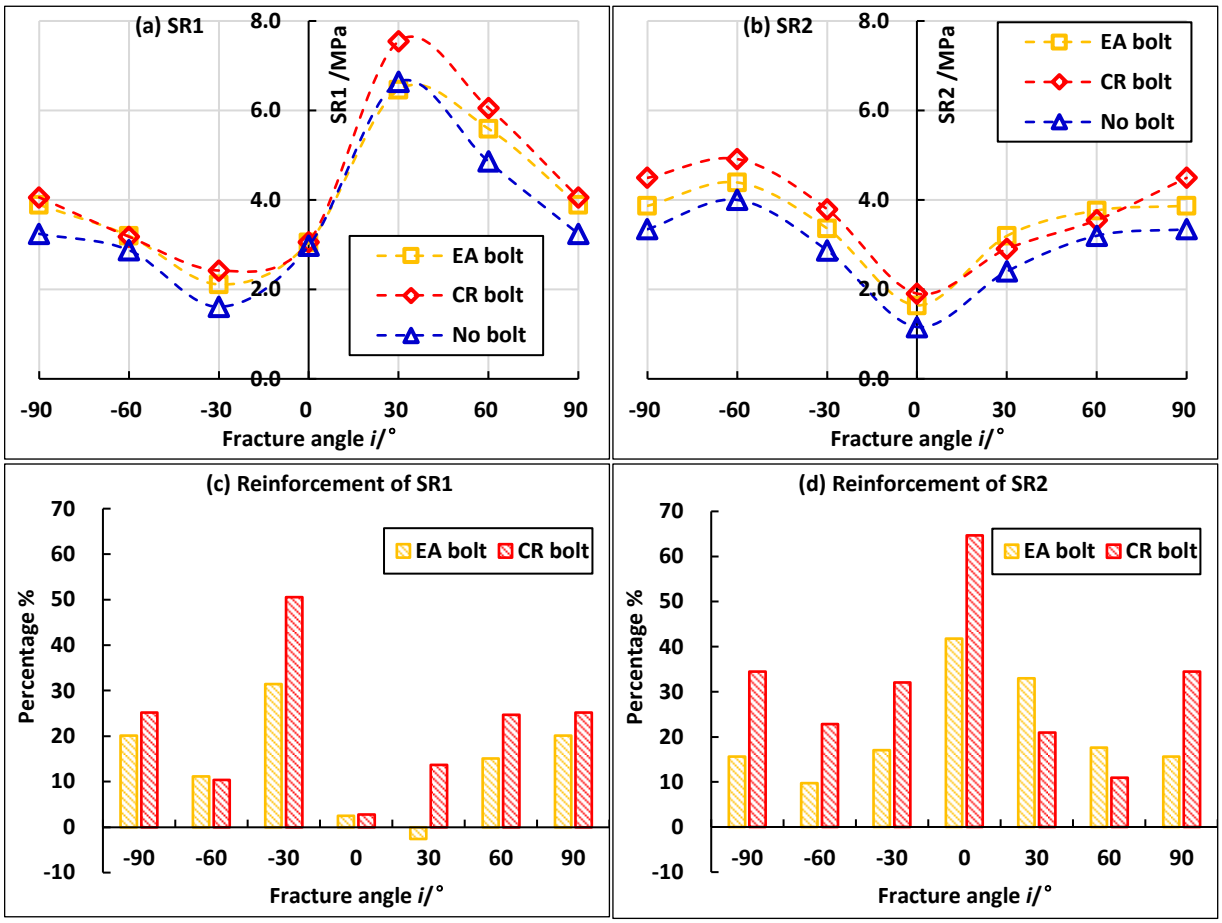

Fig. 10 Shear strength characteristics of bolted en-echelon fractures
(EA bolt: energy-absorbing bolt, CR bolt: conventional rigid bolt)

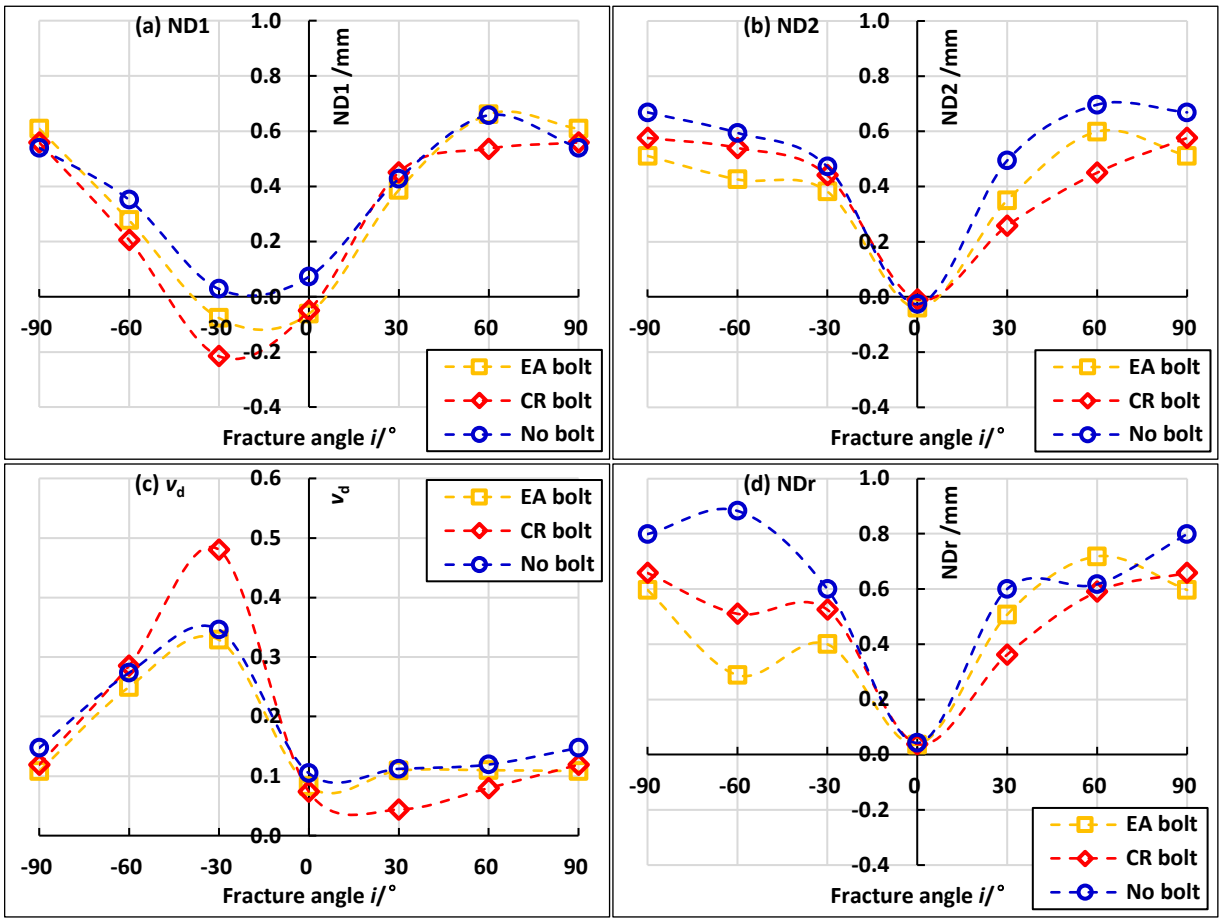

Fig. 11 Dilation characteristics of bolted en-echelon fractures
(EA bolt: energy-absorbing bolt, CR bolt: conventional rigid bolt)

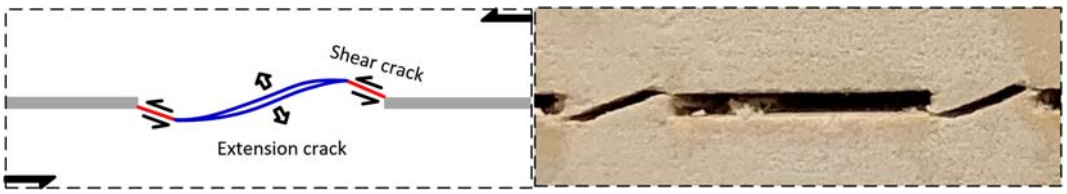

(a) Planar failure structure

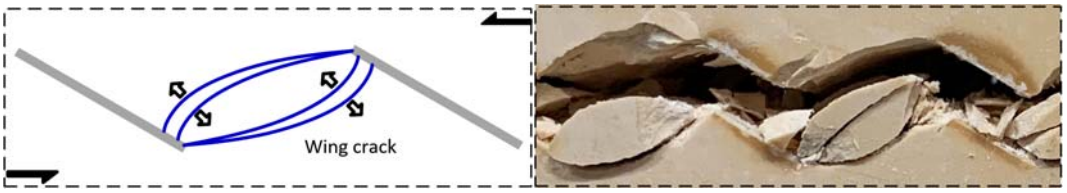

(b) Sawtooth failure structure

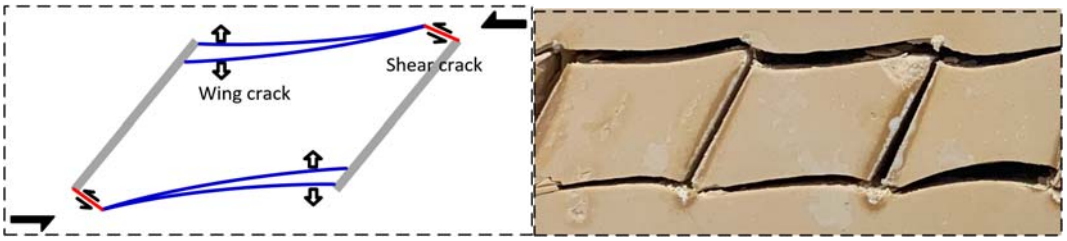

(c) Block failure structure

Fig. 12 Three typical shear failure structures evolved from en-echelon fractures

(a) *i*=-30° Sawtooth failure (Rigid bolt)

(b) *i*=-30° Sawtooth failure (Energy-absorbing bolt)

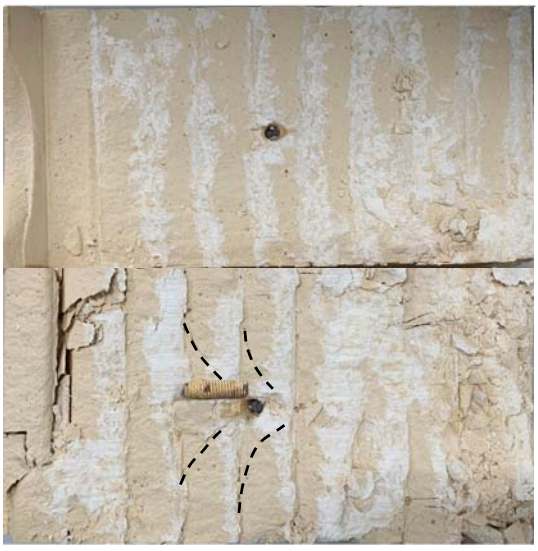

(c) *i*=60° Block failure (Rigid bolt)

(d) *i*=60° Block failure (Energy-absorbing bolt)

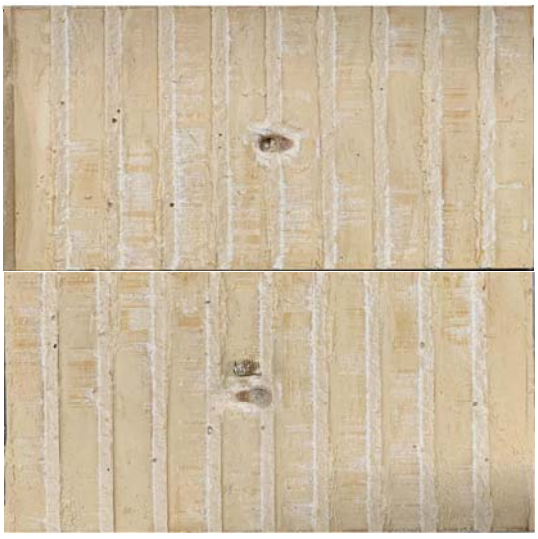

(e) *i*=0° Planar failure (Rigid bolt)

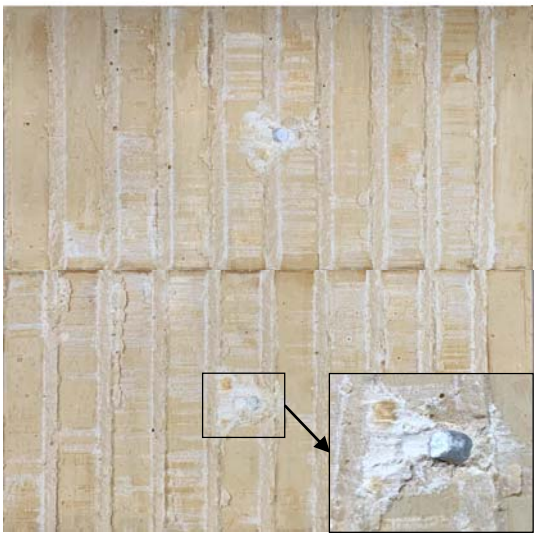

(f) *i*=0° Planar failure (Energy-absorbing bolt)

Fig. 13 Damage characteristics of bolts in different shear failure structures

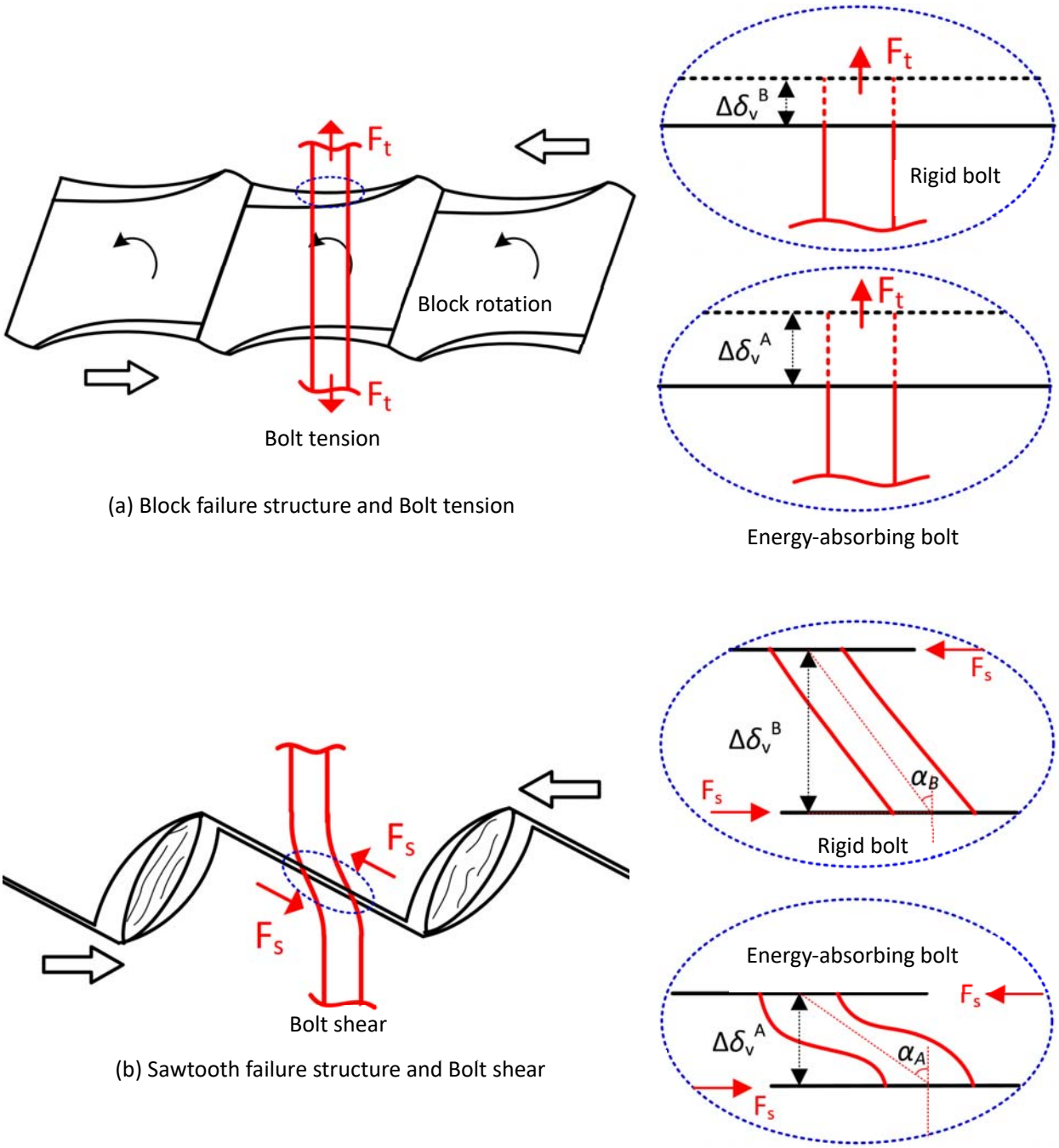

Fig. 14 Shear failure structure and bolt deformation mechanism

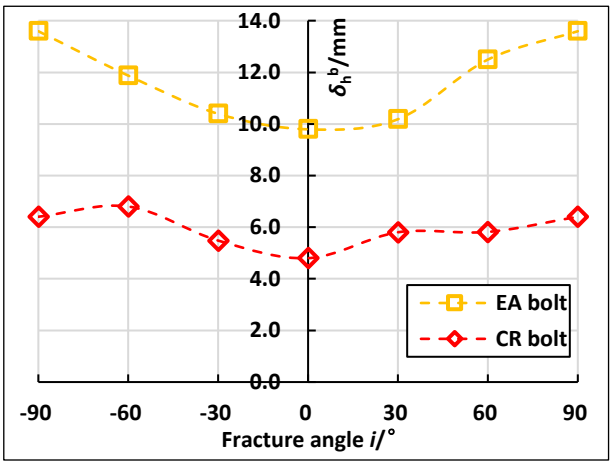

(a)

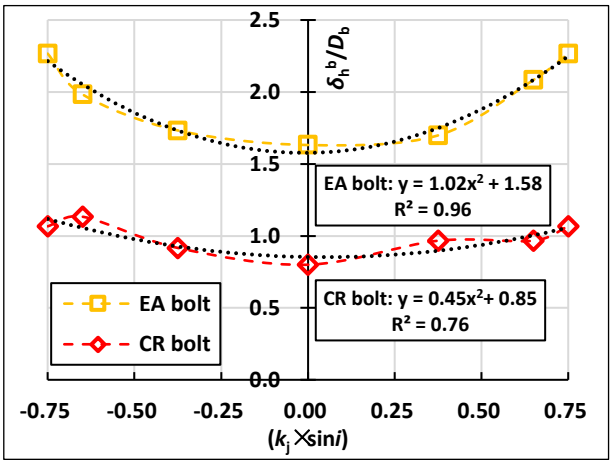

(b)

Fig. 15 Variation of bolt breakage displacement (a) and dimensionless treatment (b).
(EA bolt: energy-absorbing bolt, CR bolt: conventional rigid bolt)

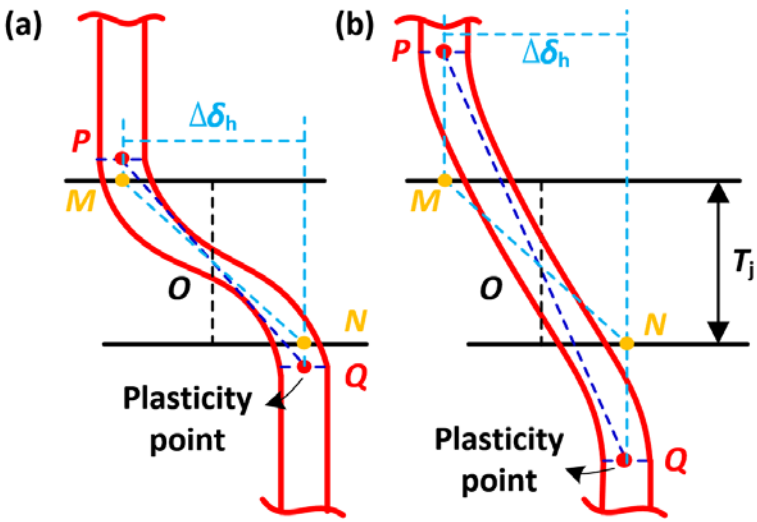

Fig. 16 Definition of bolt deformation parameters. (a) Energy-absorbing bolt (b) Rigid bolt

i=0° *i*=30° *i*=-30° *i*=60° *i*=-60° *i*=90°

(a) Rigid bolt

i=0° *i*=30° *i*=-30° *i*=60° *i*=90°

(b) Energy-absorbing bolt

Fig. 17 Measurement of L_{PQ} value of bolts.

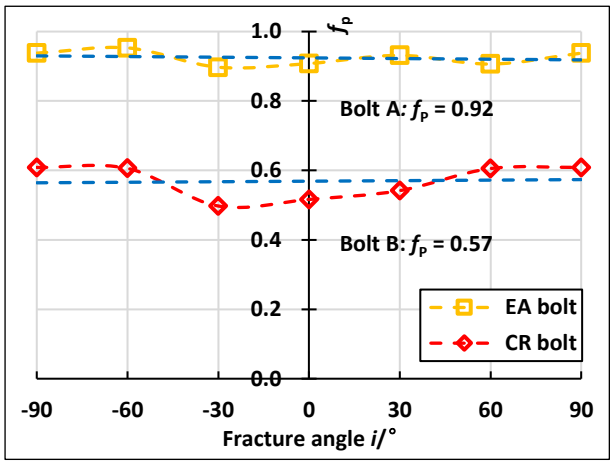

(a)

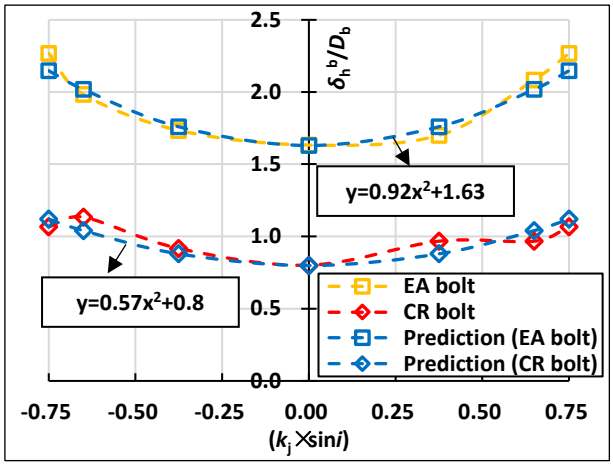

(b)

Fig. 18 Bolt deformation factors (a) and prediction of breakage displacement (b).

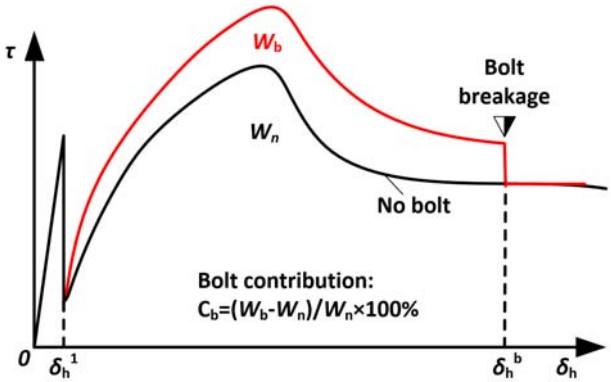

(a)

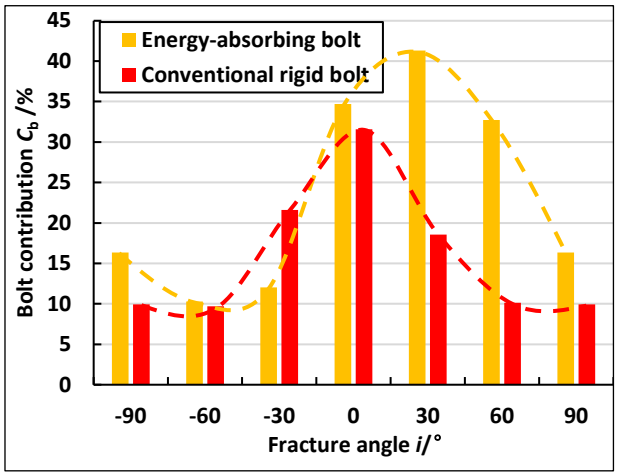

(b)

Fig. 19 Definition (a) and comparison (b) of bolt contribution.